Geochemistry, Geophysics, Geosystems®

AGU ADVANCING EARTH AND SPACE SCIENCE

RESEARCH ARTICLE
10.1029/2021GC009742

Key Points:

- Noise-based velocity variation measurements are explained by modeled water levels inside an aquifer
- Geodetic evidence of elastic and poroelastic response of the zone to the rainfall
- Identification of the effect of seismic active period in the velocity variations

Supporting Information:

Supporting Information may be found in the online version of this article.

Correspondence to:

A. Barajas,
custore@gmail.com

Citation:

Barajas, A., Poli, P., D'Agostino, N., Margerin, L., & Campillo, M. (2021). Separation of poroelastic and elastic processes of an aquifer from tectonic phenomena using geodetic, seismic, and meteorological data in the Pollino region, Italy. *Geochemistry, Geophysics, Geosystems*, *22*, e2021GC009742. https://doi.org/10.1029/2021GC009742

Received 3 MAR 2021
Accepted 19 OCT 2021

Separation of Poroelastic and Elastic Processes of an Aquifer From Tectonic Phenomena Using Geodetic, Seismic, and Meteorological Data in the Pollino Region, Italy

Andrés Barajas[1], Piero Poli[1], Nicola D'Agostino[2], Ludovic Margerin[3], and Michel Campillo[1]

[1]ISTerre, Grenoble, France, [2]INGV, Rome, Italy, [3]IRAP, Toulouse, France

Abstract Velocity variations obtained from ambient seismic noise are sensitive to many factors. We aimed to disentangle these processes in a 10-year-long recording of seismic noise from a single station in the Pollino region, in southern Italy. This region is characterized by aquifers and by a relatively short period of high seismic activity that included slow slip events and a M_W 5.0 earthquake that occurred on October 25, 2012. We apply two models that estimate the water level inside an aquifer, which show a good correlation with the measured $\delta v/v$, showing that the velocity variations are inversely proportional to the pore pressure inside the aquifer. Our interpretation is further confirmed by geodetic measurements that show that in a direction parallel to the strike angle of the fault rupture, the expansion-contraction displacement of the zone follows the same patterns observed in the models and in the velocity variations, as a result of the pressure generated by the water on its interior. Going one step further, we analyze the nature of the small discrepancies between the measured and modeled velocity variations. These correlate well with the rainfall and with the vertical geodetic measures, which indicates an elastic response of the zone to the loading generated by the rainwater. Comparisons between these variables allow us to clearly identify the period of the seismic activity in the zone, which is represented by the characteristic drop in the seismic velocity in the period from the beginning of 2012 to mid-2013.

1. Introduction

Analysis of ambient seismic noise (Campillo, 2006; Campillo & Paul, 2003; Shapiro & Campillo, 2004) has allowed estimation of changes in the velocities in the crust related to a variety of phenomena, such as earthquakes (Brenguier, Campillo, et al., 2008), volcanic activity (Brenguier, Shapiro, et al., 2008; Rivet et al., 2015), and the thermoelastic responses of the soil (Meier et al., 2010), among others. Many studies have focused on the hydrological effects on the $\delta v/v$. Sens-Schönfelder and Wegler (2006) estimated the underground water levels using a model developed by Akasaka and Nakanishi (2000), to define the direct relations to the measured velocity variations in a volcano. Meier et al. (2010) analyzed velocity variations within the Los Angeles basin (USA), and concluded that the seasonal variations are strongly influenced by groundwater level changes and thermo-elastic strain variations. Clements and Denolle (2018) found a direct correlation between velocity variations measured through seismic noise and measurements of the ground-water level. Tsai (2011) proposed periodic models to recreate displacement and velocity changes from thermo-elastic stress and hydrological loading. Wang et al. (2017) reported a direct relation between velocity variations and several hydrological and meteorological processes across Japan, which were mainly based on the pore pressure generated by rainwater through a diffusion process. Hillers et al. (2014) showed a correlation between velocity changes and periodicity of precipitation events in Taiwan.

Hydrological deformation processes have also been studied through geodetic data (Bawden et al., 2001; Borsa et al., 2014; Chanard et al., 2014; Watson et al., 2002). In general, the effects of rainfall can be seen in two ways: as an elastic response where the water exerts a loading pressure that subsides the surface (Amos et al., 2014; Argus et al., 2014; Nof et al., 2012); or as a poroelastic response that generates a rise in the surface as a consequence of the recharging of the porous inner structure of the soil (Galloway & Burbey, 2011; King et al., 2007).

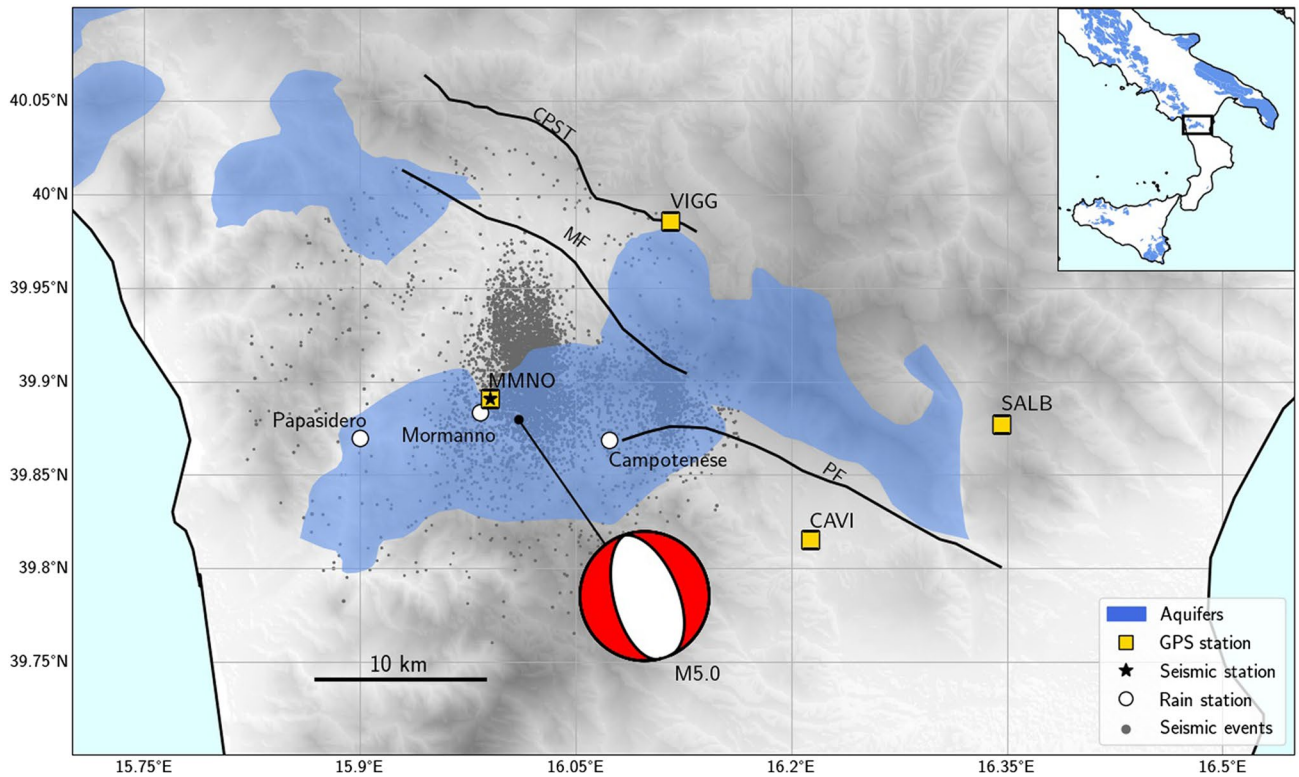

Figure 1. General disposition of the seismic, rain and GPS stations, and location of the aquifers and the M_W 5.0 earthquake, in the study area in Calabria, Italy. The CPTS, MF and PF lines represent the Castello Seluci-Timpa della Manca, Mercure, and Pollino faults, respectively (Michetti et al., 2000; Papanikolaou & Roberts, 2007). The rain data was obtained from the Multi-risk Functional Centre (ARPACAL, 2021).

From the aforementioned studies, it emerges that the thermal and hydrological effects on $\delta v/v$ are significant, and these can thus mask velocity changes induced by tectonic processes. It is therefore fundamental to quantify such environmental effects, to resolve the velocity variations induced by tectonic processes in studies of the physics of faults. Examples of this approach include the study of Hillers et al. (2019), where seasonal variations were filtered out, to highlight deformation patterns of tectonic origin around the San Jacinto fault (USA), and the study of Poli et al. (2020), where tectonic and hydrological processes were separated from a single station analysis of $\delta v/v$. In the present study, we pursue this same objective: we disentangle the influence of the water content inside the crust from the tectonic events.

One of the main characteristics of this zone is the presence of karst aquifers, which are likely to be the driving factor behind the non-steady, transient behavior found in seismic velocity measurements and geodetic displacements (D'Agostino et al., 2018; Poli et al., 2020). The highest precipitation of the zone usually happens between November and February, with low to moderate rainfall in the summer. In this region is present the massif Pollino where temperatures can greatly vary depending on the altitude that can be up to 2267 m. This area was relatively inactive seismically until the beginning of 2012, when a seismic swarm began that lasted until the middle of 2013, a period that included several earthquakes, such as a M_W 5.0 event on October 25, 2012 (Passarelli et al., 2015). It has been estimated that 75 percent of 6000 events detected during the swarms were not aftershocks, which means that the driving mechanism behind the swarm might be a transient forcing. The physical nature of this transient forcing might be fluid filtration, pore pressure diffusion, or aseismic slow slip (Parotidis et al., 2003; Peng & Gomberg, 2010). This last scenario can also be associated with fluid-related phenomena that can reduce the normal stress in the fault. It has also been suggested that a large part of the crustal deformation in the zone arises through transient slow slip events (Cheloni et al., 2017).

In this study, we measure the seismic velocity variation $\delta v/v$ in the Pollino region, Italy (Figure 1), from ambient seismic noise recorded by a single station over nine years. We determine the role of the water in the

$\delta v/v$ measurements by comparing them with two different models that calculate the water levels inside an aquifer based on recordings of the rainfall. Based on these models, the contribution of the water inside the aquifer to the $\delta v/v$ is estimated. The interpretation of the mechanism through which the water in the aquifer controls the velocity variations is consistent with independent horizontal geodetic measurements that show an expansion-contraction behavior of the region with the same characteristics of the seismic measurements and the modeled water contents in the aquifer. Afterward, the modeled velocity variation produced by the stored water in the aquifer is removed from the seismic measurements, allowing the analysis of other phenomena that are also present in seismic records. A weaker pattern is identified, mainly controlled by the immediate elastic response of the zone to the rainfall, which is also the main driving factor behind the variations in the vertical geodetic measurements. Finally, this procedure reveals a velocity drop that is most probably related to the stress release of the zone through seismic activity.

2. Data Processing

The overall layout of the data-collection stations is shown in Figure 1. The seismic ambient noise was recorded at station MMNO in the Pollino area (Italy) (INGV Seismological Data Centre, 2006). The three-component continuous signals are band-passed between 0.5 Hz and 1.0 Hz. For each day, the whole signal is divided into overlapping windows of 30 min each (50% overlap). We then calculate the cross-correlation between the 30-min windows for all the possible combinations of the three available channels. This means that for each 30-min segment, we obtain six cross-correlations. In practice, we calculate these simultaneously using the Covnet package (Seydoux et al., 2017). The 30-min cross-correlations are averaged for each day, which results in six cross-correlations per day. Afterward, to stabilize the signals obtained and to reduce possible transient noise sources, the correlations are replaced by the moving average of correlations within a window of 30 days around each day. Finally, six global reference cross-correlations are obtained by averaging all the available correlations. Variations in the velocity can be estimated if we consider that a perturbation in the medium will generate a change in the shape of the daily cross-correlation with respect to the global average, in the same way that a pulse emitted in the position of the seismic station would be registered differently if the velocity of the medium change. We calculate this possible change with the Moving Window Cross Spectral analysis (Poupinet et al., 1984) using the segment of the coda of the cross-correlations between 10 s and 50 s. We assume that the phenomena we want to observe do not depend on the direction of the seismic field and therefore, the six different combinations are averaged between them daily to decrease the level of noise in the measurements. Finally, a moving average of 30 days is applied over the resulting $\delta v/v$ series.

The GPS displacements were obtained from rinex data of GNSS stations belonging to the Rete Integrata Nazionale GPS network (Istituto Nazionale di Geofisica e Vulcanologia INGV, 2016). These data were processed using the Jet Propulsion Laboratory GIPSY-OASIS II software following the procedure used in D'Agostino et al. (2018).

The rain data were collected from the three closest stations available, as shown in Figure 1. Data were not available for all the study period from all the three stations, so an averaging process was carried out for each day using the available information for that day. This provides an estimation of the regional daily rainfall, which is shown in Figure 2a.

Figure 2b shows the accumulated seismic moment per day in a radius of $15km$ around the station MMNO, and the slip-rate reported by Cheloni et al. (2017). The aseismic slip rate is estimated from a time dependent inversion over GPS observations and line-of-sight displacements derived from short repeat-time Synthetic Aperture Radar images, assuming a uniform slip on the rupture plane. The data is inverted to obtain the dimensions, positions and strike, dip and rake of the fault plane. The results of the inversion showed that the main area of transient aseismic slip took place between $2km$ and $7km$ along a source model that is consistent with the coseismic fault plane of the M_W 5.0 event on October 25, 2012 mainshock.

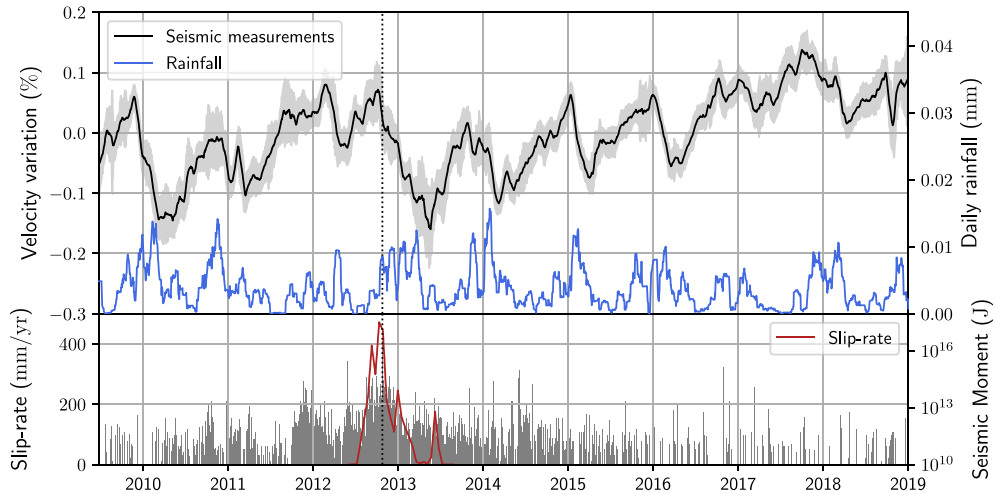

Figure 2. (a) Seismic measurements of $\delta v/v$ and the moving average of the daily rainfall in the region calculated over a window of 30 days. The gray area represents the measurements error calculated by the Moving Window Cross Spectral analysis. (b) Daily accumulated seismic moment in the region, and slip-rate as reported by Cheloni et al. (2017). The dashed line indicates the date of the M_W 5.0 seismic event.

3. Procedure and Results

3.1. Measured and Modeled Velocity Variations

The noise-based velocity variations shown in Figure 2a reveal several patterns. There is a periodic (1 year) oscillation that appears to be related to the amount of water in the crust (i.e., the regional daily rainfall). Indeed, the daily rain observed on the region (Figure 2a) increases during the winter, which appears to be associated with velocity reductions (Sens-Schönfelder & Wegler, 2006). Beyond the periodic signal, a long-term trend of increasing velocity is observed over the full study after 2014 (Figure 2a).

To separate the hydrological signals from the effects of possible changes in tectonic stress in the seismic $\delta v/v$ series, the induced velocity variations generated by the water in the crust are modeled. For this, we developed and applied two different models that estimate the accumulated water inside the aquifer as a function of time.

The aquifer is recharged by the rainfall through a rapid process that is due to the characteristic permeable material of the karst. We assume that this happens at a higher velocity than for normal diffusion processes: the rainfall is added each day directly to the water level of the aquifer. The discharge process can be described by two different models, both of which are related to the stored water inside the aquifer.

The first model, as a linear reservoir (Fiorillo, 2011), assumes that the aquifer loses water through flux with its surroundings at a discharge rate dQ/dt (where Q is the stored volume of water) that is proportional to the difference in the amount of water between the interior and the exterior of the karst $\Delta\phi$, and the contact area between the two A_L

$$\frac{dQ}{dt} = U A_L \Delta\phi + R \tag{1}$$

where R is any external source supplying the aquifer, and U has the role of a conductance over the surface, that is, the proportionality constant between the flux of water leaving the aquifer (per unit area) and the difference in the amounts of water; indeed, U is the equivalent of the heat transfer coefficient in the heat transfer Newton's law of cooling. From this point of view, this parallels the obtaining of Newton's law of cooling from the heat equation, which is also defined as a diffusive process. The total amount of water inside the aquifer can be defined in terms of its density and the volume it occupies. The water in the aquifer accumulates at its bottom, and therefore, this volume can be defined in terms of the area of the bottom A_B and the height of the column of water h. On the other hand, we assume that the area that transmits water is just the lateral one (with no difference in the amount of water flux at the top or the bottom). Then, the contact

area can be defined as approximately the product of the perimeter P and the height of the column of water $A_L = P * h$. Introducing these changes into the discharge equation turns it into

$$\frac{d\,(A_B h)}{dt} = U\,P h \Delta\phi + R \tag{2}$$

which means that the rate at which the aquifer loses water is proportional to the water level itself

$$\frac{dh(t)}{dt} = -kh(t) + r \tag{3}$$

where h is the water level inside the aquifer, r is the source term defined in terms of the change it generates in the water level inside the aquifer, and $k = U\,P\Delta\phi/A_B$, which depends on the geometry of the aquifer and the conductance of the medium.

The second model, as the Torricelli reservoir (Fiorillo, 2011), assumes that the aquifer works as a container that loses water through spring-loading at its bottom. The velocity at which the water leaves the aquifer is proportional to the square root of the height of the water it contains, as stated by Torricelli's law

$$v = \sqrt{2gh} \tag{4}$$

where g is gravity. In this case, the discharge can be defined in terms of this velocity and the area through which the water escapes (A_s)

$$\frac{dQ}{dt} = A_s v + R = A_s\sqrt{2gh} + R \tag{5}$$

If we define the volume of water inside the aquifer again as $A_B h$, the change in the water level will follow the same mathematical structure

$$\frac{dh(t)}{dt} = -k'\sqrt{h(t)} + r \tag{6}$$

where $k' = A_s\sqrt{2g}/A_B$, and r is the source that supplies the aquifer in terms of the water level. The constants in both of these equations are related to the physical characteristics of the aquifer, and modifying them changes the strength and the delay of the discharge for a given amount of water inside the aquifer.

Therefore, the water level each day will be the level of the day before, plus the level gained by the rainfall on that day r, minus the losses that are calculated according to the model:

$$h_{i+1} = h_i - k f(h_i) + r_i \tag{7}$$

Here, $f(h_i)$ is the particular functional dependence of the model on the water level, as defined by Equations 3 or 6. It must be noted that none of the two models take into account other possible factors that may increase or decrease the total amount of water in the aquifer, like evapotranspiration.

The units of the water level obtained by the models are the same as the units of the rainfall, which is measured as *mm* water recollected per square meter. This means that recollecting the totality of the indicated rainfall (which is most probably not the case), will produce the water levels estimated by the models only if we have an aquifer of exactly $1m^2$. Furthermore, if the area that collects the water (i.e., the area of the aquifer) is different from the area that supplies the rainwater, the proportionality between these two units will not be 1-to-1. This implies that both models allow us to estimate relative changes in the water level, but not its absolute value. However, this is not a problem, as will become clear below.

If the water level controls the velocity variation, the resulting series for h should show the same behavior as $\delta v/v$; or in other words, they will have a linear relationship. The value of the constant k in each model that optimizes the linear relation between these can be defined through the following grid search:

1. A value of k is chosen, and using the rain data as the input, the water level time series is calculated following the recursive formula of Equation 7
2. The water level is shifted toward zero, which removes its time average (represented by$\langle\cdot\rangle$):

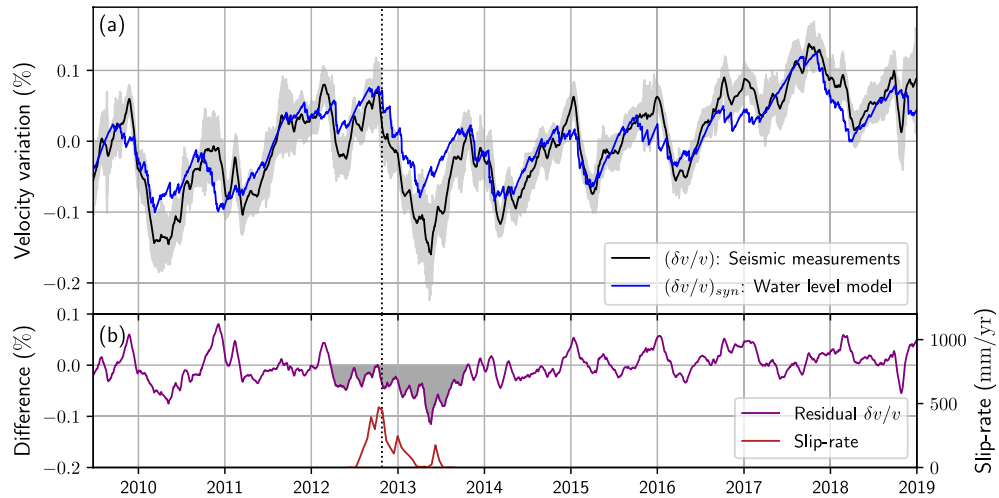

Figure 3. Seismic noise measurements and water level model. (a) Seismic and synthetic $\delta v/v$ obtained from the water level model. The gray area represents the measurements error calculated by the Moving Window Cross Spectral analysis. (b) Difference between the model and the measured $\delta v/v$ smoothed with a 30-day window and the reported slip-rate from Cheloni et al. (2017). The shaded zone highlights the systematic excess of velocity reduction between the seismic $\delta v/v$ and the rain-based model. The dashed line marks the date of the M_W 5.0 seismic event.

$$h(t) \rightarrow h(t) - \langle h(t) \rangle \tag{8}$$

3. The proportionality constant between $(\delta v/v)(t)$ and the water level time series is calculated as the ratio between the covariance and the variance: $a = \mathrm{cov}\left((\delta v/v)(t), h(t)\right)/(\mathrm{v,a,r},(h(t))$ (Rivet et al., 2015).
4. The shift or intercept between the two series is estimated as the average of the seismic velocity variation: $b = \langle (\delta v/v)(t) \rangle$
5. A synthetic velocity variation $\delta v/v_{syn}$ is obtained from the water level model using both constants a and b:

$$\frac{\delta v}{v}_{syn}(t) = \langle \frac{\delta v}{v}(t) \rangle + \left(\frac{\mathrm{cov}\left(\frac{\delta v}{v}(t), h(t) \right)}{\mathrm{var}(h(t))} \right) \cdot h(t) \tag{9}$$

6. For a given constant k, the fit to the data of the model to describe the seismic velocity variation is measured as

$$\sigma^2(k) = \frac{1}{n} \sum_{i=1}^{n} \left(\frac{\delta v}{v}(i) - \frac{\delta v}{v}_{syn}(i,k) \right)^2 \tag{10}$$

7. The process is repeated for a whole set of values of k, and the $\frac{\delta v}{v}_{syn}$ with the lowest σ^2 (the most similar to the measured $\frac{\delta v}{v}$) is chosen.

The models produce almost indistinguishable results because the daily input will only highlight any linear dependence in the long term. The misfit of each model and a comparison between them are given in Supporting Information S1. The synthetic velocity variation obtained with the linear reservoir model for the best-fit constant can be seen in Figure 3a; this will be the model used in the rest of this paper. In both cases, the covariance between the seismic measurements and the water level model is negative, which means that they are anti-correlated: an increase in the amount of water in the aquifer results in a decrease in the seismic velocity in the medium. This happens because the presence of water increases the pore pressure, which in turn reduces the overall effective pressure in the zone, and therefore reduces the seismic velocity. We can see that the models accurately reproduce the seismic-based series, not only for its seasonal patterns, but also for the overall multi-year trend, which means that the water content in the aquifer is effectively the main driving factor behind the recorded velocity variations and that the water is being accumulated within the sensitivity range of the analyzed frequency of the seismic waves. The positive trend observed

from 2014 to 2019 is a regional multi-annual hydrological trend that is also observed in the spring discharge and in the modulation of the seismicity along the Irpinia Fault (D'Agostino et al., 2018). The change in relative amplitude and phase between the rain and the water level model is illustrated in the Figure S3 in Supporting Information S1.

The difference between the measured velocity changes and the modeled velocity changes can be seen in Figure 3b. There is a periodic misfit between these, which means that a small part of the seismic velocity variation is not explained by our models. This might be due to a defect in the model or to the presence of a second phenomenon that acts in parallel with the water accumulation. Furthermore, the most remarkable feature of this difference is a systematic excess of velocity reduction, which starts at the beginning of 2012, when there was high seismic activity, and lasts approximately until the end of 2014. Here, the velocity changes measured in the seismic field are not completely accounted for by the water level model, that is, by the accumulated water that can increase the hydraulic head and the aquifer pore pressure. Although the 30-day moving average applied over the time series makes it difficult to define specific dates, this systematic difference appears to be generated by tectonic stress release, as it happens simultaneously with the seismic activity. Furthermore, through 2013, this difference appears to increase, having its maximum peak around the same time as the last pulse of the reported slow slip in the zone. It was shown that this late slip happened simultaneously with an enlargement of the crustal area affected by the seismicity (Cheloni et al., 2017). However, the systematic difference with our model extends for several months beyond the slow slip event. This extended behavior might be related to the stress change produced by the continuous low intensity seismicity which may drop the velocity variation in the same way as registered by Brenguier, Campillo, et al. (2008) for big seismic events. It is also possible that the earthquake or the slow slip changed the internal structure of the aquifer, which would produce a migration of water that might temporarily change the water level. Whatever the cause here, the changes in the velocity are completely recovered by the end of 2013.

3.2. Analysis of the Geodetic Data

Geodetic measurements are useful to measure displacements related to earthquakes and to slow slip events, and also to analyze hydrological processes inside aquifers (Cheloni et al., 2017; D'Agostino et al., 2018; Silverii et al., 2016).

We turned to an analysis of GPS traces as an independent way to assess the modeled variation of the velocity and its possible mechanisms. For this, we used GPS traces obtained from four stations in the study area, as shown in Figure 1.

The GPS displacements show trends produced by the movement of the underlying tectonic plate movement. One possibility to overcome this problem would be to detrend each of the GPS displacements with the mean displacement calculated from a group of stations. However, different stations would result in different mean trends, which means that the final result would depend on the choice of stations to include in the analysis. We use the relative displacements between stations, as they are independent of the reference frame and reflect only the deformation between the two stations.

We begin by analyzing the relative displacement between the two stations closest to the earthquake, VIGG and MMNO, with smoothing with the same 30-day window as for the velocity variation. Both of the relative horizontal components are shown in Figure 4a. To simplify the visualization of the GPS traces, they have all been shifted vertically toward zero without modifying their behavior or their relative values. This does not affect our analysis, as we are interested in the patterns described by the traces and not in their absolute values. The relative displacement shows seasonal patterns in all the directions and a clear change in the baseline due to the M_W 5.0 event.

Perhaps the most interesting feature of the traces in Figure 4a is the behavior of the NS component from 2014 until the end of the series, as it shows a similar pattern to that observed in the $\delta v/v$: a yearly seasonal variation over a multiyear increasing behavior, with approximately the same shape. However, this behavior is not seen in the EW direction. There are two reasons why this behavior is not seen for both components. One of these is a possible anisotropic response of the aquifer to the hydrostatic pressure in the horizontal direction (Silverii et al., 2016). Commonly, a porous medium like an aquifer has fractures that can open

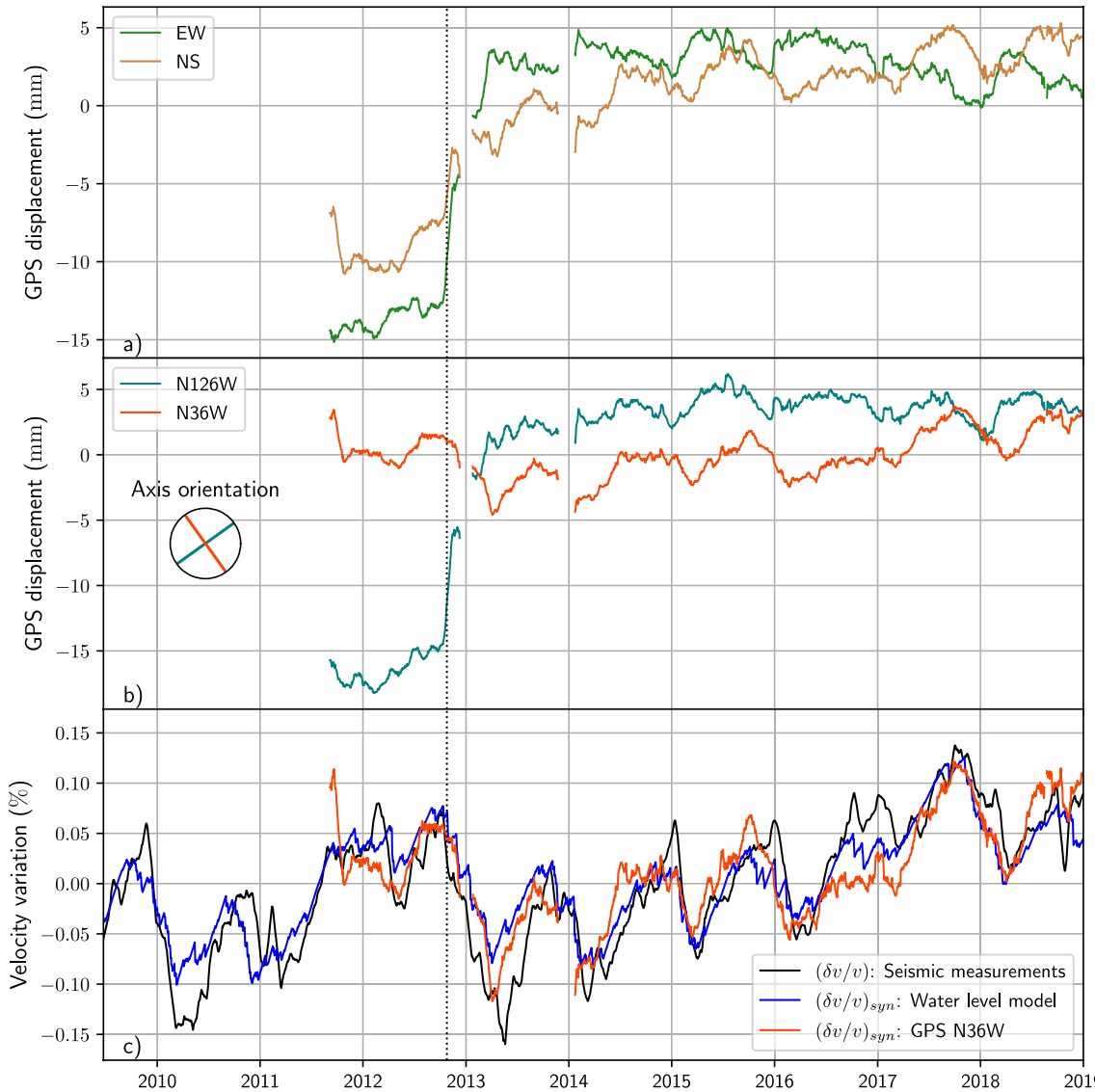

Figure 4. Modeled velocity variations and GPS relative displacements. (a) Relative horizontal GPS displacements between stations MMNO and VIGG. (b) GPS horizontal relative displacements rotated by an angle of 36° in a counterclockwise direction. (c) Velocity variations measured through seismic noise analysis, as estimated from the water level model, and fitted with the rotated $N36W$ horizontal displacement. The dashed line indicates the date of the $M_W 5.0$ seismic event.

and close temporarily according to the pressure generated by the water (Amoruso et al., 2014; Daniele et al., 2012). If these fractures lie predominately in a specific direction, the macroscopic expansion-contraction dynamics will be more (or only) visible in this direction, which constitutes an anisotropic response. Another possible reason might simply be the relative position of the GPS station to the aquifer: for example, if we had a GPS station at the north of a perfectly circular aquifer, we would expect to see the expansion-contraction recorded only in the NS component and not in the EW component, even in an isotropic fracture system.

Most likely, the main expansion-contraction direction is not exactly NS. With this in mind, a rotation is performed for the horizontal GPS traces, to find the angle that maximizes the presumed linear relation between the GPS displacement and the modeled water level inside the aquifer. This is done through a similar grid search between one rotated component of the GPS and the measured seismic $\delta v/v$, as described at the end of Section 3.1.

Figure 4b shows the rotated GPS at the best fit angle. The reason why this angle minimizes the fit can be seen in Figure 4c: the trace in the direction N36W shows the same behavior as the modeled velocity variations for all times, even in the period in which the earthquake and the slow slip occurred. There are two reasons why this trace follows the water level in the aquifer so well. The first is that the direction of this rotated GPS is the only direction in which the fault rupture of the earthquake is not visible; that is, the direction of the strike angle of the earthquake. This is important, as any other direction will show a discontinuity in the horizontal expansion of the aquifer. On the other hand, it is possible that the localization of the GPS station, which is NW of the aquifer, helps to accentuate the expansion-contraction process in that specific direction.

Beyond the mechanism that accentuates one direction in particular, it is clear that the behavior of the displacements is related to the variations seen in both the velocity changes and in the water model, which is coherent with an expansion-contraction poroelastic dynamic in the aquifer (Amoruso et al., 2014; Chaussard et al., 2014; Ojha et al., 2019). As the aquifer stretches between the four GPS stations, this process should be visible using different combinations of the stations, and not only between VIGG and MMNO. In effect, calculation of the relative displacement between all the other paired stations, and finding of the best rotation for each case, produces a similar pattern, as can be seen in Figure 5. Although different GPS combinations fit better around different angles, all the combinations that involve station MMNO (the closest to the seismic event) are maximized around 36°, possibly as a consequence of finding the projection that does not show the effect of the earthquake itself. Moreover, it can be seen that different station pairs produce different levels of intensity between the seismic event and the water-driven pattern. This indicates a possible new way to analyze the complexity of the system, and particularly the directions of the volumetric expansion of the area.

4. Loading Effect of the Rainfall

A deeper inspection of the seismic velocity variations can be made if we analyze the part of it that is not controlled by the water level in the aquifer. This can be done by subtracting one from another, as is shown in Figure 6a. This is the same difference to that shown in Figure 3, but processed with a longer moving average window of 180 days, calculated over each day, to stabilize the fluctuations and highlight the seasonal patterns. The longer smoothing window and the representation of the difference between the measured and modeled velocity variations explains why the amplitude of the pattern obtained is around 20 percent of the original amplitude of the velocity. As was seen in Figure 3, this residual velocity is not in phase with the modeled water level in the aquifer. However, a quick inspection of the rainfall smoothed over the same moving average window of 180 days (Figure 6b) reveals that both are in phase, which means that the observed behavior probably comes from the loading that the rainfall generates over the surface. This conclusion is confirmed by the vertical component of the GPS stations in the regions that show a negative correlation between the rainfall itself and the height of the surface (Figure 6c) (Amos et al., 2014; Argus et al., 2014; Nof et al., 2012). Although the three measurement series in Figures 3a–3c, are in phase, their relative amplitudes are different, even between the two GPS vertical displacements. This is probably due to particularities of the local structure around each of the stations and to differences in the surface size to which seismic changes and the GPS respond when a loading is applied. The long smoothing window helps to extract the common long-term regional behavior of the vertical GPS components, filtering out the local response of each station. As would be expected, when the rainfall increases, the loading in the area increases, which generates a positive residual velocity variation, and at the same time, produces downward motion of the vertical position (Lecocq et al., 2017; Meier et al., 2010). This is consistent with regional observations made by Silverii et al. (2016), where they reported correlation between the vertical GPS data and the Gravity Recovery and Climate Experiment satellite observations.

This implies that the responses of the crust to the rain occur in two ways: in the first, the water generated by the rainfall accumulates in the aquifer, and as a result, it produces expansion of the area that is recorded by the horizontal GPS. This is a poroelastic reaction. In the second, the rainfall generates a load over the area that is measured by the vertical GPS motion. This is an elastic reaction. Although both of these mechanisms act simultaneously, they have peaks that are not in phase (see Figures 4c and 6c), and they are each measured with different intensities by the velocity variations of the seismic noise.

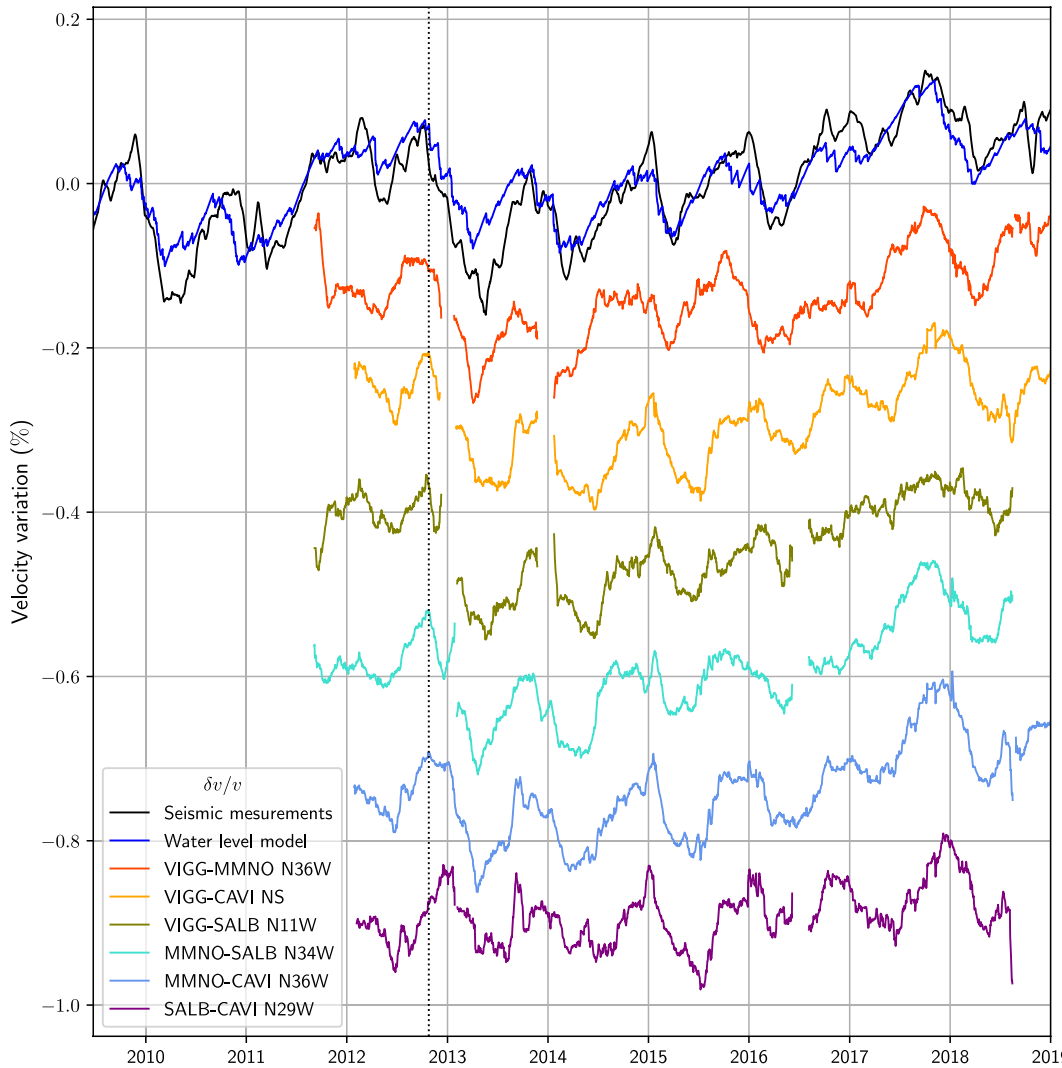

Figure 5. Comparisons between the measured velocity variations (black) and all the synthetic velocity variations obtained with the water level model (blue line) and with rotation of the GPS relative displacements for all the possible combinations between the four stations. A shift of 0.15% was introduced between these for clarity of presentation. The angle of the rotation that maximizes the fit for each couple is indicated in the key (bottom left), except for VIGG-CAVI, where no rotation was needed. The dashed line indicates the date of the M_W 5.0 seismic event.

Finally, Figure 6 shows a highlighted period in which the pattern measured in the velocity variation does not match the seasonal loading. The most probable cause of this mismatch is the simultaneous high seismic activity in the area, including the M_W 5.0 earthquake, which occurs almost in the middle of the recorded anomaly in the velocity variation. All of this is coherent with the temporary velocity drop that dominates this period, which suggests stress release within the medium (Brenguier, Campillo, et al., 2008).

5. Conclusions

To disentangle the influence of the water content inside the crust from tectonic related events, we measured the variations in seismic velocity over 10 years in the Pollino region, Italy, for a single seismic station. These show yearly oscillations that are characteristic of seasonal factors and are superimposed over a multi-year pattern. As the water content in the soil is usually one of the main factors in the control of such velocity variations, we use here two models that estimate the water level inside an aquifer in the area, with the assumption that it is recharged by rainfall and that it loses water through two different mechanisms. Both of

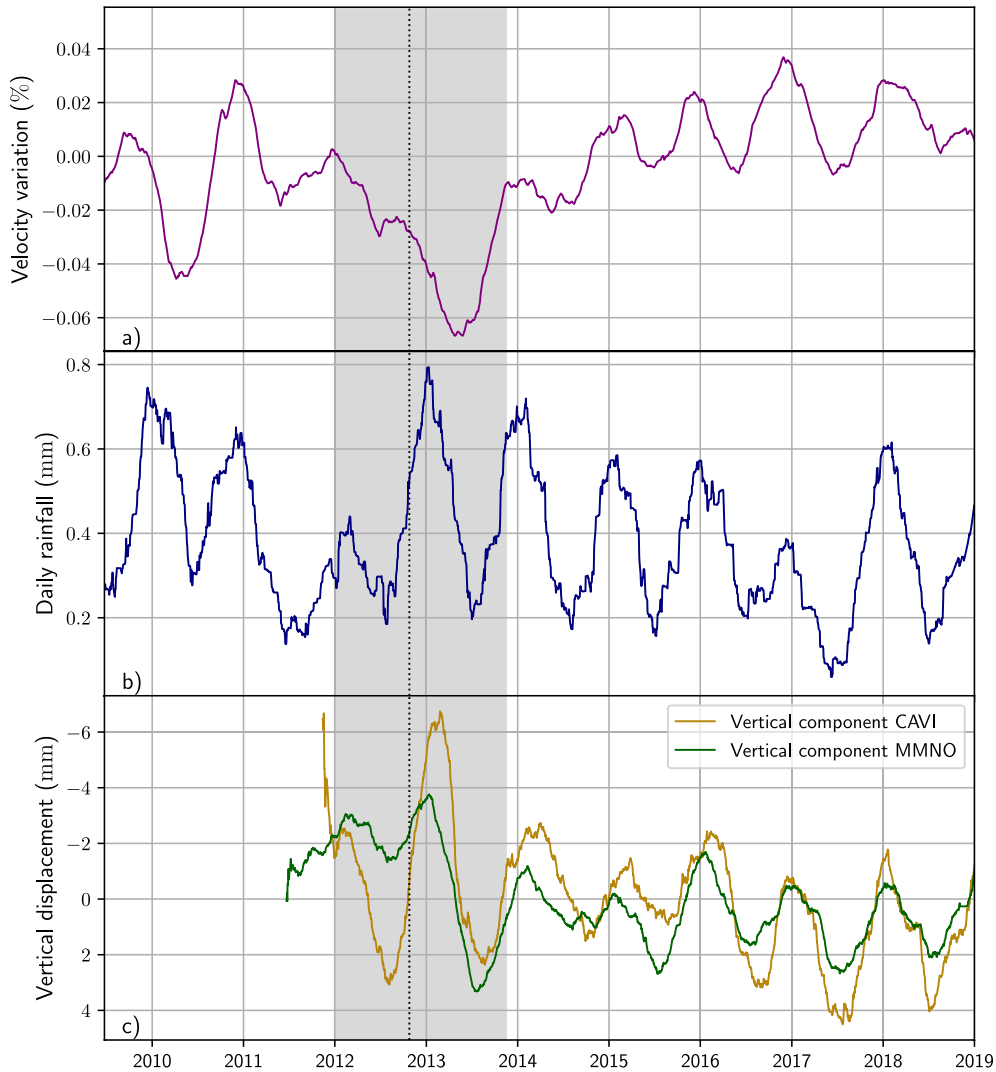

Figure 6. (a) Difference between the measured velocity variation in the seismic noise and the velocity variation of the water level model. (b) Rainfall. (c) Vertical GPS displacements of stations MMNO and CAVI (with the vertical axis inverted). The shading highlights the period for which the velocity variation is not explained by the water content of the soil, and is not in phase with the regional rainfall. The dashed line marks the date of the M_W 5.0 seismic event. All the plots are smoothed with a 180-day window.

these models use constants where the values depend on the geometric particularities of the aquifer, which are unknown. Thus, we perform a grid search to compare the resulting water level models with the velocity variations, for different constants. This comparison recreates a modeled velocity variation that essentially modifies the overall amplitude and mean of the water level, to match those of the measured velocity variation, with the calculation of the root-mean-square error between the two models. Both of the models provide a good correlation with the velocity variations, showing that increase the levels of water in the aquifer decreases the velocity of the seismic waves. The increase in pore pressure as a consequence of the aquifer water leads to a reduction in the effective pressure in the medium, and therefore to a reduction in the seismic velocity. The models recreate the yearly seasonal behavior and the long multi-year trends. This shows that the total water inside the aquifer changes slowly, and is influenced by long-lasting periods of heavy rain or drought. The comparisons between the models and the measured $\delta v/v$ also show a systematic discrepancy between them that lasts for 1–2 years, during which the seismic measurements show that the velocity on the area is lower than estimated by the model. This occurs in the same period as a M_W 5.0 earthquake, where slow slip events occur (Cheloni et al., 2017). This suggests that the velocity drop discrepancy

is produced by stress release in the tectonic system through the seismic activity and the transient aseismic deformation. This difference disappears by the end of 2013.

The NS component of the relative displacement between the VIGG and MMNO GPS stations across the fault suggests that the deformation in this area occurs synchronously with both the $\delta v/v$ and the water level of the aquifer for the period after the seismic activity that occurred between 2012 and 2013. The relative displacement in the $N36W$ direction follows the same behavior as both the measured and modeled velocity variations for the whole period that was recorded with GPS. This can be explained by the opening and closing of the fractures of the porous media under the pressure generated by the water, which generates the overall displacements recorded by the GPS. This behavior is also seen between all the other station pairs that are located in the study area. It also confirms our assumption of a poroelastic recharge and discharge process of the aquifer, upon which we base the water level models. The angle at which this occurs for the station pairs that include the MMNO station is always around 36°, which is close to the angle of the strike fault of the M_W 5.0 event (24°), possibly because for this direction the sharp displacement generated by the earthquake is minimized. Moreover, the angles that maximize this expansion-contraction mechanism for the station pairs that are not close to the earthquake (i.e., VIGG-CAVI, VIGG-SALB, CAVI-SALB) show interesting differences that appear to be related to the shape of the aquifer or to local anisotropic behavior.

Subtraction of the modeled velocity variations generated by the water level inside the aquifer from the observed seismic velocity variations reveals a pattern of weaker amplitude that is in phase with the regional rainfall. The vertical displacements of the GPS in the study area are also closely negatively correlated with the rainfall. This indicates an elastic behavior of the area that occurs in parallel with the described poroelastic dynamics. Thus, the rainfall generates a loading over the surface that results in subsidence of the elevation of the area (and therefore the negative correlation with the vertical GPS), and in a small increase in the stress of the crust (and therefore an increase in the seismic velocity), which are reflected in the $\delta v/v$.

Finally, this procedure highlights a period in which an anomalous velocity drop breaks the in-phase behavior between the residual seismic velocity and both the rainfall and the vertical GPS. This occurs simultaneously with a period of high seismic activity of the area, which includes a M_W 5.0 earthquake. Therefore, the velocity drop appears to be related to the stress release associated with the seismic activity of the area. This means that our analysis allows us to extract the seismic signature of the tectonic stress release despite two environment processes, that is, the elastic and poroelastic responses to the precipitation, that occur simultaneously and dominate the variations in the seismic velocity.

Data Availability Statement

The seismic data can be downloaded at Instituto Nazionale di Geofisica e Vulcanologia (https://doi.org/10.13127/SD/X0FXNH7QFY). The RINEX daily files from RING GPS stations can be accessed at http://ring.gm.ingv.it. The rain data were provided by the Centro Funzionale Multirischi of the Calabria region (http://www.cfd.calabria.it/).

Acknowledgments
ERC F-image - This project has received funding from the European Research Council (ERC) under the European Union Horizon H2020 Research and Innovation program (grant agreement No 742335). The authors wish to thank Qing-Yu Wang and Francesco Fiorillo for the insightful discussions, and the constructive comments from the anonymous reviewers.

References

Akasaka, C., & Nakanishi, S. (2000). Correction of background gravity changes due to precipitation: Oguni geothermal field, Japan. In *Proceedings world geothermal congress* (pp. 2471–2475).

Amoruso, A., Crescentini, L., Martino, S., Petitta, M., & Tallini, M. (2014). Correlation between groundwater flow and deformation in the fractured carbonate Gran Sasso aquifer (INFN underground laboratories, central Italy). *Water Resources Research*, *50*(6), 4858–4876. https://doi.org/10.1002/2013WR014491

Amos, C. B., Audet, P., Hammond, W. C., Bürgmann, R., Johanson, I. A., & Blewitt, G. (2014). Uplift and seismicity driven by groundwater depletion in central California. *Nature*, *509*(7501), 483–486. https://doi.org/10.1038/nature13275

Argus, D. F., Fu, Y., & Landerer, F. W. (2014). Seasonal variation in total water storage in California inferred from GPS observations of vertical land motion. *Geophysical Research Letters*, *41*(6), 1971–1980. https://doi.org/10.1002/2014GL059570

ARPACAL. (2021). *Centro funzionale multirischi della Calabria*. Retrieved from http://www.cfd.calabria.it/

Bawden, G. W., Thatcher, W., Stein, R. S., Hudnut, K. W., & Peltzer, G. (2001). Tectonic contraction across Los Angeles after removal of groundwater pumping effects. *Nature*, *412*(6849), 812–815. https://doi.org/10.1038/35090558

Borsa, A. A., Agnew, D. C., & Cayan, D. R. (2014). Ongoing drought-induced uplift in the western United States. *Science*, *345*(6204), 1587–1590. https://doi.org/10.1126/science.1260279

Brenguier, F., Campillo, M., Hadziioannou, C., Shapiro, N. M., Nadeau, R. M., & Larose, E. (2008). Postseismic relaxation along the San Andreas fault at Parkfield from continuous seismological observations. *Science*, *321*(5895), 1478–1481. https://doi.org/10.1126/science.1160943

Brenguier, F., Shapiro, N. M., Campillo, M., Ferrazzini, V., Duputel, Z., Coutant, O., & Nercessian, A. (2008). Towards forecasting volcanic eruptions using seismic noise. *Nature Geoscience*, *1*(2), 126–130. https://doi.org/10.1038/ngeo104

Campillo, M. (2006). Phase and correlation in 'random' seismic fields and the reconstruction of the Green function. *Pure and Applied Geophysics*, *163*(2), 475–502. https://doi.org/10.1007/s00024-005-0032-8

Campillo, M., & Paul, A. (2003). Long-range correlations in the diffuse seismic coda. *Science*, *299*, 547–549. https://doi.org/10.1126/science.1078551

Chanard, K., Avouac, J. P., Ramillien, G., & Genrich, J. (2014). Modeling deformation induced by seasonal variations of continental water in the Himalaya region: Sensitivity to Earth elastic structure. *Journal of Geophysical Research: Solid Earth*, *119*(6), 5097–5113. https://doi.org/10.1002/2013JB010451

Chaussard, E., Bürgmann, R., Shirzaei, M., Fielding, E. J., & Baker, B. (2014). Predictability of hydraulic head changes and characterization of aquifer-system and fault properties from insar-derived ground deformation. *Journal of Geophysical Research: Solid Earth*, *119*(8), 6572–6590. https://doi.org/10.1002/2014jb011266

Cheloni, D., D'Agostino, N., Selvaggi, G., Avallone, A., Fornaro, G., Giuliani, R., et al. (2017). Aseismic transient during the 2010-2014 seismic swarm: Evidence for longer recurrence of M ≥ 6.5 earthquakes in the Pollino gap (Southern Italy)? *Scientific Reports*, *7*(1), 576. https://doi.org/10.1038/s41598-017-00649-z

Clements, T., & Denolle, M. A. (2018). Tracking groundwater levels using the ambient seismic field. *Geophysical Research Letters*, *45*(13), 6459–6465. https://doi.org/10.1029/2018GL077706

D'Agostino, N., Silverii, F., Amoroso, O., Convertito, V., Fiorillo, F., Ventafridda, G., & Zollo, A. (2018). Crustal deformation and seismicity modulated by groundwater recharge of karst aquifers. *Geophysical Research Letters*, *45*(22), 12253–12262. https://doi.org/10.1029/2018GL079794

Daniele, T., Braitenberg, C., & Nagy, I. (2012). Karst deformations due to environmental factors: Evidences from the horizontal pendulums of Grotta Gigante, Italy. *Bollettino di Geofisica Teorica Applicata*, *53*, 331–345. https://doi.org/10.4430/bgta0049

Fiorillo, F. (2011). Tank-reservoir drainage as a simulation of the recession limb of karst spring hydrographs. *Hydrogeology Journal*, *19*, 1009–1019. https://doi.org/10.1007/s10040-011-0737-y

Galloway, D., & Burbey, T. (2011). Review: Regional land subsidence accompanying groundwater extraction. *Hydrogeology Journal*, *19*, 1459–1486. https://doi.org/10.1007/s10040-011-0775-5

Hillers, G., Campillo, M., Brenguier, F., Moreau, L., Agnew, D. C., & Ben-Zion, Y. (2019). Seismic velocity change patterns along the San Jacinto fault zone following the 2010 M7.2 El Mayor-Cucapah and M5.4 Collins Valley earthquakes. *Journal of Geophysical Research: Solid Earth*, *124*(7), 7171–7192. https://doi.org/10.1029/2018JB017143

Hillers, G., Campillo, M., & Ma, K.-F. (2014). Seismic velocity variations at TCDP are controlled by MJO driven precipitation pattern and high fluid discharge properties. *Earth and Planetary Science Letters*, *391*, 121–127. https://doi.org/10.1016/j.epsl.2014.01.040

INGV Seismological Data Centre. (2006). *Italian national seismic network*. Istituto Nazionale di Geofisica e Vulcanologia (INGV). https://doi.org/10.13127/SD/X0FXnH7QfY

Istituto Nazionale di Geofisica e Vulcanologia, INGV. (2016). *Rete integrata nazionale gps (ring)*. Istituto Nazionale di Geofisica e Vulcanologia INGV. https://doi.org/10.13127/RING

King, N. E., Argus, D., Langbein, J., Agnew, D. C., Bawden, G., Dollar, R. S., et al. (2007). Space geodetic observation of expansion of the San Gabriel Valley, California, aquifer system, during heavy rainfall in winter 2004 2005. *Journal of Geophysical Research*, *112*(B3), B03409. https://doi.org/10.1029/2006JB004448

Lecocq, T., Longuevergne, L., Pedersen, H. A., Brenguier, F., & Stammler, K. (2017). Monitoring ground water storage at mesoscale using seismic noise: 30 years of continuous observation and thermo-elastic and hydrological modeling. *Scientific Reports*, *7*(1), 14241. https://doi.org/10.1038/s41598-017-14468-9

Meier, U., Shapiro, N. M., & Brenguier, F. (2010). Detecting seasonal variations in seismic velocities within Los Angeles basin from correlations of ambient seismic noise. *Geophysical Journal International*, *181*(2), 985–996. https://doi.org/10.1111/j.1365-246X.2010.04550.x

Michetti, A. M., Ferreli, L., Esposito, E., Porfido, S., Blumetti, A. M., Vittori, E., & Roberts, G. P. (2000). Ground effects during the 9 September 1998, Mw = 5.6 Lauria earthquake and the seismic potential of the "aseismic" Pollino region in Southern Italy. *Seismological Research Letters*, *71*(1), 31–46. https://doi.org/10.1785/gssrl.71.1.31

Nof, R., Ziv, A., Doin, M.-P., Baer, G., Fialko, Y., Wdowinski, S., & Bock, Y. (2012). Rising of the lowest place on Earth due to Dead Sea water-level drop: Evidence from SAR interferometry and GPS. *Journal of Geophysical Research*, *117*, B05412. https://doi.org/10.1029/2011JB008961

Ojha, C., Werth, S., & Shirzaei, M. (2019). Groundwater loss and aquifer system compaction in San Joaquin valley during 2012–2015 drought. *Journal of Geophysical Research: Solid Earth*, *124*(3), 3127–3143. https://doi.org/10.1029/2018jb016083

Papanikolaou, I. D., & Roberts, G. P. (2007). Geometry, kinematics and deformation rates along the active normal fault system in the southern Apennines: Implications for fault growth. *Journal of Structural Geology*, *29*(1), 166–188. https://doi.org/10.1016/j.jsg.2006.07.009

Parotidis, M., Rothert, E., & Shapiro, S. A. (2003). Pore-pressure diffusion: A possible triggering mechanism for the earthquake swarms 2000 in Vogtland/NW-Bohemia, central Europe. *Geophysical Research Letters*, *30*(20), 2075. https://doi.org/10.1029/2003GL018110

Passarelli, L., Hainzl, S., Cesca, S., Maccaferri, F., Mucciarelli, M., Roessler, D., et al. (2015). Aseismic transient driving the swarm-like seismic sequence in the Pollino range Southern Italy. *Geophysical Journal International*, *201*(3), 1553–1567. https://doi.org/10.1093/gji/ggv111

Peng, Z., & Gomberg, J. (2010). An integrated perspective of the continuum between earthquakes and slow-slip phenomena. *Nature Geoscience*, *3*(9), 599–607. https://doi.org/10.1038/ngeo940

Poli, P., Marguin, V., Wang, Q., D'Agostino, N., & Johnson, P. (2020). Seasonal and coseismic velocity variation in the region of L'Aquila from single station measurements and implications for crustal rheology. *Journal of Geophysical Research: Solid Earth*, *125*(7), e2019JB019316. https://doi.org/10.1029/2019JB019316

Poupinet, G., Ellsworth, W. L., & Frechet, J. (1984). Monitoring velocity variations in the crust using earthquake doublets: An application to the Calaveras Fault, California. *Journal of Geophysical Research: Solid Earth*, *89*(B7), 5719–5731. https://doi.org/10.1029/JB089iB07p05719

Rivet, D., Brenguier, F., & Cappa, F. (2015). Improved detection of preeruptive seismic velocity drops at the Piton de La Fournaise volcano. *Geophysical Research Letters*, *42*(15), 6332–6339. https://doi.org/10.1002/2015GL064835

Sens-Schönfelder, C., & Wegler, U. (2006). Passive image interferometry and seasonal variations of seismic velocities at Merapi Volcano, Indonesia. *Geophysical Research Letters*, *33*(21), L21302. https://doi.org/10.1029/2006GL027797

Seydoux, L., de Rosny, J., & Shapiro, N. M. (2017). Pre-processing ambient noise cross-correlations with equalizing the covariance matrix eigenspectrum. *Geophysical Journal International*, *210*(3), 1432–1449. https://doi.org/10.1093/gji/ggx250

Shapiro, N. M., & Campillo, M. (2004). Emergence of broadband Rayleigh waves from correlations of the ambient seismic noise. *Geophysical Research Letters*, *31*(7), L07614. https://doi.org/10.1029/2004GL019491

Silverii, F., D'Agostino, N., Métois, M., Fiorillo, F., & Ventafridda, G. (2016). Transient deformation of karst aquifers due to seasonal and multiyear groundwater variations observed by GPS in southern Apennines (Italy). *Journal of Geophysical Research: Solid Earth*, *121*(11), 8315–8337. https://doi.org/10.1002/2016JB013361

Tsai, V. C. (2011). A model for seasonal changes in GPS positions and seismic wave speeds due to thermoelastic and hydrologic variations. *Journal of Geophysical Research*, *116*(B4), B04404. https://doi.org/10.1029/2010JB008156

Wang, Q. Y., Brenguier, F., Campillo, M., Lecointre, A., Takeda, T., & Aoki, Y. (2017). Seasonal crustal seismic velocity changes throughout Japan. *Journal of Geophysical Research: Solid Earth*, *122*(10), 7987–8002. https://doi.org/10.1002/2017JB014307

Watson, K. M., Bock, Y., & Sandwell, D. T. (2002). Satellite interferometric observations of displacements associated with seasonal groundwater in the Los Angeles basin. *Journal of Geophysical Research*, *107*(B4). ETG 8–1–ETG 8–15. https://doi.org/10.1029/2001JB000470